Highlights of Spanish Astrophysics XI, Proceedings of the XV Scientific Meeting of the Spanish Astronomical Society held on September 4–9, 2022, in La Laguna, Spain. M. Manteiga, L. Bellot, P. Benavidez, A. de Lorenzo-Cáceres, M. A. Fuente, M. J. Martínez, M. Vázquez- Acosta, C. Dafonte (eds.), 2023

AB Aur: A Rosetta stone for planet formation theories. System chemistry.

Rivière-Marichalar, P.[1], Fuente, A.[1], Navarro-Almaida, D.[1,2], Baruteau, C. [3], and Le Gal, R.

[1] Observatorio Astronómico Nacional (OAN,IGN), Calle Alfonso XII, 3. 28014 Madrid, Spain
[2] Département d'Astrophysique (DAp), Commissariat à l'Énergie Atomique et aux Énergies Alternatives (CEA), Orme des Merisiers, Bât. 709, 91191 Gif sur Yvette, Paris-Saclay, France
[3] IRAP, Université de Toulouse, CNRS, UPS, Toulouse, France
[4] Institut de Radioastronomie Millimétrique, 300 rue de la Piscine, F-38406 Saint-Martin d'Hères, France

Abstract

AB Aur is a Herbig Ae star that hosts a well-known protoplanetary disk in which a series of interesting features are observed. Such features (a large inner cavity, a dust trap, and spiral arms) can be attributed to the presence of a forming planet, making AB Aur an interesting target to study planet formation and the interactions between a disk and a forming planet. We present NOEMA observations of molecular species towards the transition disk around AB Aur, including CO, ^{13}CO, C^{18}O, HCN, HCO$^+$, SO, H_2CO, and H_2S. These observations reveal a complex chemistry with strong chemical differentiation in the radial and azimuthal directions and the presence of a cavity-crossing filament. We have computed a series of Nautilus models to help us interpret our observations. Our astrochemical models point to a disk with a low gas-to-dust ratio and strong sulfur depletion. These Nautilus models helped us to understand the sulfur budget in the disk and the role of sulfuretted species in the system chemistry, and more generally in planet-forming disks.

1 Introduction

Planets are born in circumstellar disks made of gas and dust that surround young stellar objects, implying that a planet's composition is, at least partially, inherited from the protoplanetary disk. Therefore, characterizing the physical conditions and the chemical composition of protoplanetary disks is key for understanding planet formation. Furthermore, to study the chemical complexity of planetary atmospheres, it is mandatory to understand that of protoplanetary disks.

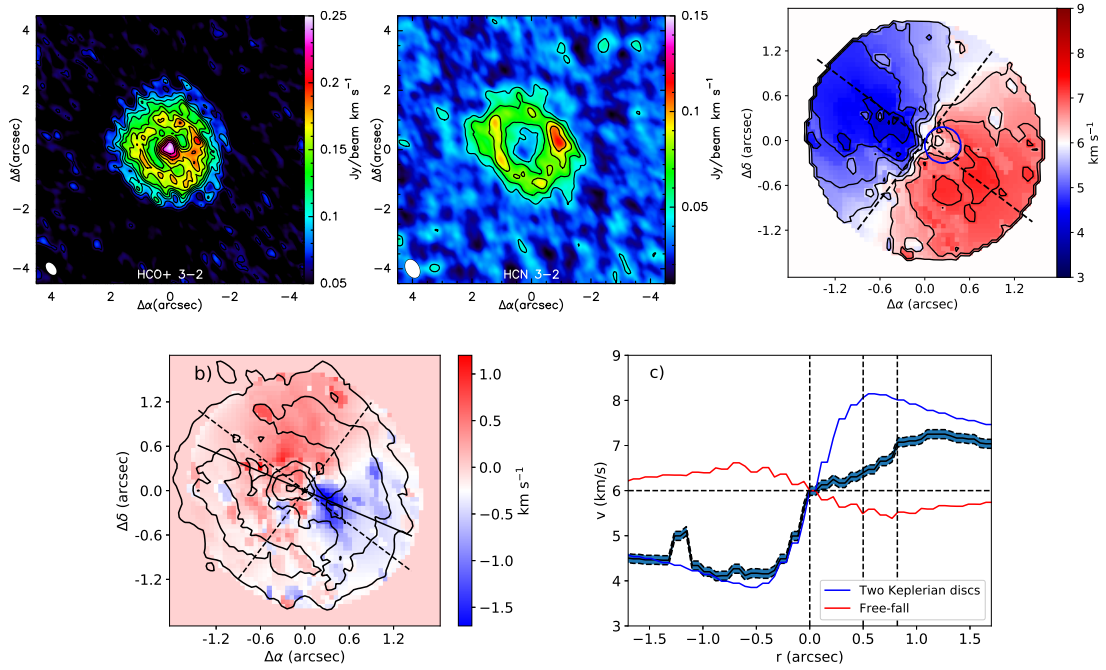

Figure 1: Top: from left to right we show the velocity-integrated intensity maps of HCO^+ (left) and HCN (right) 3-2 emission, and the HCO^+ 3-2 first-moment map. In the HCO^+ 3-2 first-moment map, the dashed lines indicate the direction of the major and minor axes. The blue circle contains a region with large anomalies with respect to a Keplerian rotation velocity field. The synthesized beam is shown in the bottom left corner of each map. Bottom: from left to right we show the residuals of a model consisting of two Keplerian disks and a cut along the velocity anomaly for the HCO^+ first-moment map (black lines with dashed region). Solid contours in the left panel depict 5σ to 25σ levels of the integrated line intensity. The black solid line shows the direction of the cut through the bridge used for the right panel. In the right panel, the blue line depicts a model consisting on two Keplerian disks (blue line), and a free-falling component (red line). The dashed vertical lines mark the positions of the center, the bridge, and the inner edge of the dust disk. From [30].

Statistical studies are key to understanding planet formation, but the detailed characterization of individual sources can provide deep insights into the physical properties and chemical reaction networks that are present in protoplanetary disks. AB Aur is a widely studied Herbig A0 star that hosts a transitional disk. At a distance of ∼160 pc [14], the system is well suited to study the distribution of gas and dust in circumstellar environments. The system presents a series of features that can be attributed to planet formation, such as a large inner cavity [29, 37, 38, 11], spiral arms [13, 17, 38, 31], and a dust trap [29, 11]. The source has been observed at all wavelengths from visible to centimetric. Low-resolution spectral observations are available from ∼1 μm up to ∼ 400 μm. The detection of lines of O I, C II, C, OH, as well as rovibrational lines of CO and H_2 demonstrates the existence of warm gas in the source. The origin of these emission lines is, however, uncertain due to the moderate

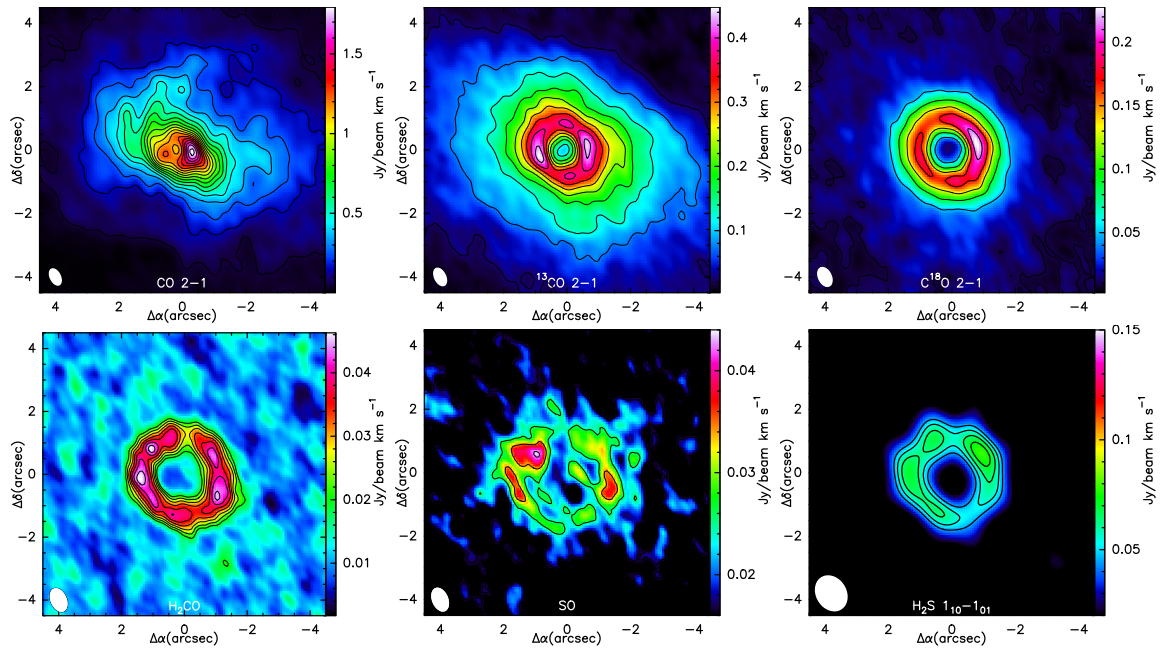

Figure 2: From left to right and top to bottom the panels show the velocity integrated intensity maps of ^{12}CO 2-1, ^{13}CO 2-1, C^{18}O 2-1, H_2CO 3_{03}-2_{02}, SO 5_6-4_5, and H_2S 1_{10}-1_{01}. The synthesized beam is shown in the bottom left corner of each map. From [31] and [32].

angular resolution of the observations. A few molecular species have been detected in AB Aur, including CO, SO, HCO^+, HCN, H_2CO, and H_2S [36, 29, 37, 38, 9, 25, 26, 30, 31, 32]. The first detection of SO in a protoplanetary disk was reported towards AB Aur [9, 25, 26]. Our team is performing a large observational effort to study the dust and gas content in this interesting object [11, 30, 31]. In this proceedings, we summarize the main results of our study.

2 NOEMA observations of HCN and HCO^+: accretion within the dust cavity?

We observed AB Aur with NOEMA in 2017 [30] to map the emission of HCO^+ 3-2 and HCN 3-2. Velocity-integrated intensity maps are shown in Fig. 2. Both maps look vey different. While HCN is detected in an annular ring spatially coincident with the dust ring, HCO^+ is detected in the outer ring and also features intense emission towards the central position. But the most striking feature of the HCO^+ 3-2 map is a bright HCO^+ emission bridge that connects the outer disk with the inner structure [30].

We show in the right panel of Fig. 2 the first-moment map of HCO^+ J=3-2. The outer parts of the disk are close to Keplerian rotation, but twisted isophotes are observed towards the center (r<0.6"). Two mechanisms have been proposed to explain twisted isophotes: two

Table 1: Peak position in radial profiles, and angle peak in azimuthal profiles of the continuum and the different species surveyed before de-projection. The last column gives the binding energy of the different species surveyed. References are: [1] [8]; [2] [24]; [3] [16]

Species –	Peak position (")	Peak position (au)	Peak. angle (°)	E_D (K)
Cont 1mm	0.96	157	269	–
^{12}CO	0.292	52	279	1575[1]
^{13}CO	0.80	130	279	1575[1]
$C^{18}O$	0.89	146	275	1575[1]
p$-H_2CO$	1.20	195	279	3260[2]
SO	1.41	229	105	2600 [3]
HCO^+	0.00	0.0	92	–
HCN	1.02	166	99	2050[3]

misaligned Keplerian disks [17] and the presence of an outflow [34]. We created a simple model consisting of two misaligned disks. This model provides a good fit across the disk except in the position of the bridge region, where prominent residuals are observed. Visual inspection of spectra at this position demonstrates the presence of material moving at forbidden velocities, most likely infalling material moving at free-fall velocities. By including a free-fall velocity component in our model we get a much better fit to the first-moment map. At the position of the bridge, the free-fall model has a velocity of 5.5 km s^{-1}, compared to the velocity of 5.3 km s^{-1} of the blue-shifted component observed towards the bridge. According to this, the material in the bridge seems to be infalling at a velocity close to free-fall. Assuming that this component was due to accretion, we derived a mass accretion rate in the range $3{\times}10^{-8}$ to $3{\times}10^{-7}$ $M_\odot$ yr^{-1}, comparable to previous measurements [35].

Radial inflows crossing dust cavities have been invoked before to explain a series of features observed in protoplanetary disks, such as gas and dust streamers and twisted isophotes [4, 7, 27, 43, 20, 21, 42]. Radial inflows were proposed to explain absorption features in CO ro-vibrational lines towards AA Tau [43], with material moving at free-fall velocities in regions between the inner and outer disk. These gap-crossing radial inflows could explain the high accretion levels derived in transitional disks, such as those observed in AB Aur [15, 35]. A compact and collimated bipolar jet was detected by [33] in the continuum at 7 mm suggesting the existence of a disk-jet system. In order to sustain it, the gas must flow through the cavity and reach the inner regions of the system. Otherwise, accretion would drain the inner disk very fast.

3 Spatial distribution of chemical species

We continued our research by studying the spatial distribution of ^{12}CO, ^{13}CO, $C^{18}O$, HCN, HCO^+, SO, H_2CO [31], and H_2S [32], by means of high angular resolution NOEMA observa-

Table 2: Nautilus 1D model parameters.

Parameter	Value
Molecular cloud	
T_{gas} (K)	10
T_{dust} (K)	10
n_H	10^4
A_v	20
f_{UV} (Draine units)	1
ζ_{H_2} (s^{-1})	10^{-17}
Gas-to-dust mass ratio	100
AB Aur at r=200 au	
T_{mid} (K)	39
T_{atm} (K)	65
A_v	2
f_{UV}(Draineunits)	1.2×10^4
ζ_{H_2} (s^{-1})	10^{-17}
Gas-to-dust mass ratio	40

tions. The species surveyed showed strong radial segregation, with differences as large as 100 au in the positions of their radial peaks. The only species that peaked toward the center was HCO^+. The emission from all gaseous species was more extended than that of the dust, ^{12}CO and ^{13}CO being the most extended ones, with 5σ emission detected at distances larger than 4" due to pollution by envelope emission. It sounds reasonable to postulate that this radially layered structure is related to the snow lines of the different species, which are determined by their binding energies. If thermal desorption is the main desorption mechanism in the mid-plane, one would expect that the radius of the snow line anti-correlates with the binding energy. However, this was not the behavior observed (see Table 2), which suggests that thermal desorption is not the main driver of the surface chemistry in this system. Furthermore, our data revealed that different species are probing different regions of the disk and the envelope. Species such as ^{12}CO and ^{13}CO trace the disk surface and the remnant envelope. Other species, such as $C^{18}O$ and HCN, are tracing the dusty disk, with a radial profile that almost overlaps with that of the continuum. H_2CO and SO trace the outer regions of the disk, and SO is likely to arise from shocked regions, such as the centrifugal barrier.

We also observed differences in the azimuthal profiles of the different species. $C^{18}O$ peaks close to the position of the dust trap, while SO peaks at $\sim180°$ from the position of the dust trap, and other species such as HCN, H_2CO, and HCO^+ are mostly flat along the ring.

Using H_2CO lines we derived a mean gas temperature of 39 K. Using SO lines we derived a temperature of 37 K, in good agreement with the value from H_2CO lines. This average temperature of 39 K is larger than the typical value for disks around T Tauri stars. By combining observations of the continuum, ^{13}CO, and $C^{18}O$ we computed a gas-to-dust ratio map, with a mean value of 40.

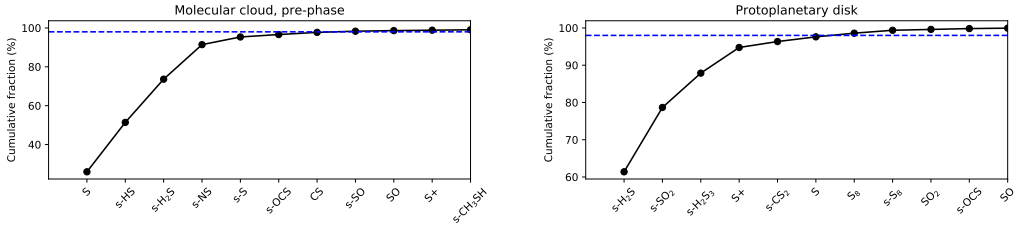

Figure 3: Cumulative sulfur abundance fraction of the ten main sulfur carriers from `Nautilus` models. Left: molecular cloud. Right: AB Aur protoplanetary disk at r=200 au. The horizontal blue dashed line depicts the position of the 98% cumulative fraction. From [32].

4 Chemical modeling and sulfur budget

To help us interpret our interferometric data, we developed a series of 1+1D Nautilus models [41], following the prescriptions used by [19]. The details of the model can be found in [31] and [19]. The elemental gas phase sulfur abundance is a controversial issue [10, 40, 39, 12, 23]. In our models, we considered a high-S abundance case, with the sulfur elemental abundance equal to the solar one [2], and a low-S case with S/H$\sim 8\times10^{-8}$, which is the value usually adopted to fit the abundances of S-bearing species in dark clouds [1]. We varied three parameters: the gas-to-dust ratio (40 and 100), the sulfur abundance (solar, [S/H]$=1.5\times10^{-5}$, and depleted, [S/H]$=8\times10^{-8}$), and the carbon to oxygen relative abundance (C/O=0.7 and C/O=1). By comparing the model abundances with that derived from our observations, we concluded that the best model was one with a low gas-to-dust ratio (thus supporting our estimated value), strong sulfur depletion ([S/H]$=8\times10^{-8}$), and C/O=1, supporting the idea that evolved disks are oxygen depleted [3, 5, 18, 22].

The previous models aimed at reproducing our observations of sulfuretted species in AB Aur. After our detection of H_2S we decided to model again the chemistry of AB Aur using Nautilus, but this time our focus was on understanding the budget of sulfur, as well as of molecular species in general. Instead of producing a 1D+1 model, we estimated the abundances at 200 au, where all the observed species are detected, allowing us to study the chemical budget and the evolution with height. The values adopted for the different parameters are summarized in Table 2. To set our initial abundances we first modeled the chemistry of a 10 K molecular cloud for 1 Myr, and used the output abundances from that model as input for the protoplanetary disk model. The parameters for the molecular cloud are also shown in Table 2. The details of the model can be found in [32].

In Fig. 3, we show the total cumulative fraction for the 10 most abundant sulfuretted species for the cold molecular cloud (left) and the AB Aur protoplanetary disk (right). In our protoplanetary disk model, 98% of the sulfur budget is contained in six species: g-H_2S, g-SO_2, g-H_2S_3, S^+, g-CS_2, and S, where g- stands for molecular species in the surface of dust grains. The budget is dominated by surface species, with 90.5% of the sulfur contained in molecular species on the surface of grains, and 9.5% in species in the gas phase. We show in Fig. 4 the 10 most abundant species for the different phases of the model. Surface H_2S

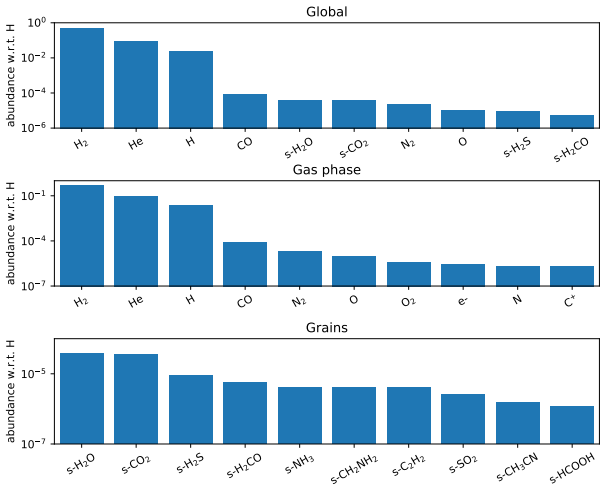

Figure 4: Abundances of the ten most abundant species in our `Nautilus` model for the global content (top), the gas phase (middle), and the surface of grains (bottom). From [32].

is the third most abundant species in the surface of grains, after H_2O and CO. Considering all phases, g-H_2S is the ninth most abundant species in the model, making H_2S a relevant component of dust grains, whose abundance in different protoplanetary systems is worth modeling to understand the chemical budget.

To test the stability of our sulfur budget model we computed new models where key parameters were changed, including the temperature of the cold cloud prephase, the UV field, the grain size, and the temperature of the mid-plane. For the temperature of the cold prephase, we computed a second model with a cloud temperature of 18 K, instead of 10 K. The abundance of all molecular species remained the same within an order of magnitude, exception made of $HSCN^+$. To test the impact of the UV -field, we computed a model with $f_{UV} = 12$ instead of $f_{UV} = 1.2 \times 10^4$, and observed that 85% of the sulfur species remained the same within an order of magnitude. To understand the role of the grain size distribution we computed a model where we assumed a different grain size at each height, with 1 mm grains in the mid-plane, 0.1 μm grains in the atmosphere, and a logarithmic interpolation in between. Again, most of the species (92%) remained the same within an order of magnitude. Finally, to test the impact of varying the mid-plane temperature we computed a model with a mid-plane temperature of 10 K. We show in the top panel of Fig. 5 the cumulative sulfur abundance fraction of the ten most relevant sulfur carriers from this model. The most relevant sulfur carrier, g-HS, is not among the 10 most abundant sulfur carriers in the original model. Most species that are important sulfur carriers in the original model are irrelevant to the sulfur budget in the 10 K model. In the mid panel of Fig. 5 we show a comparison of the abundances of all the sulfuretted species in both models. The large scatter observed indicates that varying the temperature of the mid-plane gas has an important impact on

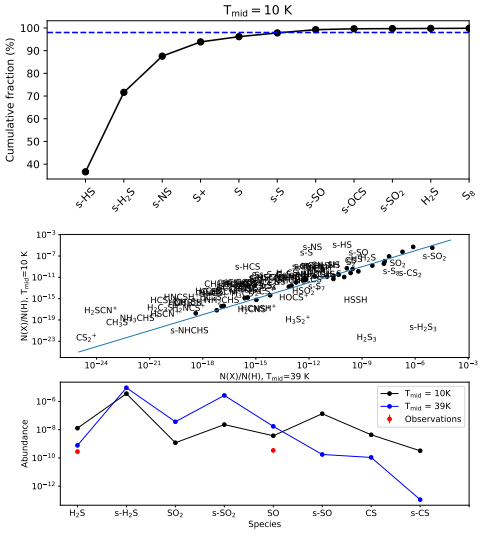

Figure 5: Impact of varying the mid-plane temperature on the model results. Top: cumulative sulfur abundance fraction of the ten main sulfur carriers for the `Nautilus` model with T_{mid}=10 K. Middle: abundance of sulfuretted species computed assuming T_{mid}=10 K versus the abundance computed assuming T_{mid}=39 K. We show the names of the species when there is an order of magnitude difference between both models, and plot black dots otherwise. Bottom: abundance of a subset of the most relevant sulfur carriers for the two mid-plane temperatures used. From [32].

the derived sulfur abundances. In the bottom panel of Fig. 5 we show the abundance of a subset of important sulfuretted species in both models. These species include H_2S, g-H_2S, SO_2, g-SO_2, SO, g-SO, CS, and g-CS. Large differences are observed, indicating the power of simultaneously observing this set of species to derive the mid-plane temperature.

5 Summary

AB Aur's protoplanetary disk presents a series of interesting phenomena that could be the result of the interaction between the disk and an embedded planet, including a cavity in the inner disk, a dust trap, and spiral arms. Thus, studying AB Aur can help us to get insight into the physical and chemical properties during the process of planet formation. For the last few years we have been driving an observational program to characterize the gaseous content of this system using observations with the NOEMA interferometer, the ALMA interferometer, and the IRAM 30 m telescope.

Our observations of HCO^+ revealed the presence of a gap crossing filament that connects the inner and outer disk. The material in this bridge appears to be moving at free-fall velocities and it is likely due to the material being accreted onto the central source. Assuming

that this component was due to accretion we derived an accretion rate in good agreement with previous estimates from the literature. Such radial inflow has been observed before and could explain the high accretion levels observed in transitional disks.

Our NOEMA observations showed strong radial segregation of chemical species in the disk. The positions of the radial peaks of the different species surveyed thus far suggest that thermal desorption is not driving the chemical evolution of the disk, and other mechanisms such as chemical desorption seem to be playing an important role. We derived an average gas-to-dust ratio of 40, significantly smaller than the value of 100 assumed for the ISM, in agreement with recent studies. We used observations our of H_2CO and SO to estimate a mean temperature of 39 K for the gas in the disk.

To help us to interpret the data, we modeled the chemical content of the protoplanetary disk using Nautilus. In our first attempt, we aimed at reproducing the abundance of the sulfuretted species detected thus far in the gas phase. Our best model was one with a gas-to-dust ratio of 40, in agreement with our estimate, strong sulfur depletion ([S/H]=8×10^{-8}), and a relative abundance of carbon to oxygen C/O=1, in agreement with recent studies that show an overabundance of carbon with respect to oxygen in evolved protoplanetary disks. After the detection of H_2S we aimed at deriving the evolution of the sulfur budget with height and to understand the role of sulfuretted species in the global chemistry of the system. According to our NAUTILUS model, H_2S is the main sulfur carrier on the surface of grains. It is also the third most abundant species on the surface of grains, after H_2O and CO_2. Our results show that H_2S observations are an essential diagnostic to determine the level of sulfur depletion in protoplanterary disks. Observations of H_2S and other sulfuretted species toward more young stellar objects are needed to understand sulfur depletion and put our observations of AB Aur in context. Our results also show the relevance of the mid-plane temperature for sulfur chemistry, illustrating to what extent the chemistry of T Tauri and HAeBe are different.

Future observations with NOEMA will help us to grow our database to study the protoplanetary disk around AB Aur and contribute to our global knowledge of the chemistry of protoplanetary systems.

Acknowledgments

PRM and AF thank the Spanish MINECO for funding support from PID2019-106235GB-I00.

References

[1] Agúndez, M. & Wakelam, V., Chemical Reviews, 113, 8710 (2013)

[2] Asplund, M., Grevesse, N., & Sauval, A. J., in Astronomical Society of the Pacific Conference Series, Vol. 336, ed. T. G. Barnes, III & F. N.Bash, 25 (2005)

[3] Bergin, E. A., Du, F., Cleeves, L. I., et al., ApJ, 831, 101 (2016)

[4] Casassus, S., van der Plas, G., M, S. P., et al. , Nature, 493, 191 (2013)

[5] Cleeves, L. I., Öberg, K. I., Wilner, D. J., et al., ApJ, 865, 155 (2018)

[6] Daflon, S., Cunha, K., de la Reza, R., et al., AJ **138**, 1577-1583 (2009)

[7] Dutrey, A., di Folco, E., Guilloteau, S., et al., Nature, 514, 600 (2014)

[8] Fayolle, E. C., Balfe, J., Loomis, R., et al., ApJL, 816, L28 (2016)

[9] Fuente, A., Cernicharo, J., Agúndez, M., et al., A&A **524**, A19 (2010)

[10] Fuente, A., Cernicharo, J., Roueff, E., et al., A&A, 593, A94 (2016)

[11] Fuente, A., Baruteau, C., Neri, R., et al., A&A **846**, L3 (2017)

[12] Fuente, A., Navarro, D. G., Caselli, P., et al., A&A, 624, A105 (2019)

[13] Fukagawa, M., Hayashi, M., Tamura, M., et al., ApJL **605**, L53-L56 (2004)

[14] Gaia collaboration, Vizier Online Data Catalog, I345 (2018)

[15] Garcia-Lopez, R., Natta, A., Testi, L., et al. A&A, 459, 837, (2006)

[16] Garrod, R. T. & Herbst, E., A&A, 457, 927 (2006)

[17] Hashimoto, J., Tamura, M., Muto, T., et al., ApJ **729**, L17 (2011)

[18] Le Gal, R., Brady, M. T., Öberg, K. I., et al., F., ApJ, 886, 86 (2019a)

[19] Le Gal, R., Öberg, K. I., Loomis, R. A., Pegues, J., & Bergner, J. B. , ApJ, 876, 72, (2019b)

[20] Loomis, R. A., Öberg, K. I., Andrews, S. M.,MacGregor, M. A., ApJ, 840, 23 (2017)

[21] Mendigutía, I., Oudmaijer, R. D.,Garufi, A., et al., A&A, 608, A104 (2017)

[22] Miotello, A., Facchini, S., van Dishoeck, E. F., et al., A&A, 631, A69 (2019)

[23] Navarro-Almaida, D., Le Gal, R., Fuente, A., et al., A&A, 637, A39 (2020)

[24] Noble, J. A., Theule, P., Mispelaer, F., et al., A&A, 543, A5 (2012)

[25] Pacheco, S., Fuente, A., Agúndez, M., et al., A&A, **578**, A81 (2015)

[26] Pacheco, S., Fuente, A., Baruteau, C., et al., A&A, **589**, A60 (2016)

[27] Perez, S., Casassus, S., Ménard, F., et al., ApJ, 798, 85 (2015)

[28] Phuong, N. T., Chapillon, E., Majumdar, L., et al., A&A **616**, L5 (2018)

[29] Piétu, V., Guilloteau, S., Durtey, A., A&A **443**, 945-954 (2005)

[30] Rivière-Marichalar, P., Fuente., A., Baruteau, C., et al., ApJL **879**, L14 (2019)

[31] Rivière-Marichalar, P., Fuente, A., Le Gal, R., et al., A&A **642**, A32 (2020)

[32] Rivière-Marichalar, P., Fuente, A., Esplugues, G., A&A **652**, A46 (2022).

[33] Rodríguez, L. F., Zapata, L., A., Dzib, S. A., et al., ApJ **793**, L21 2014

[34] Rosenfeld, K., A., Chiang, E., Andrew, S. M., ApJ **782**, 62 (2014)

[35] Salyk, C., Herczeg, G. J., Brown, J. M., et al., ApJ **769**, 21 (2013)

[36] Schreyer, K., Guilloteau, S., Semenov, D., et al., A&A, **491**, 821-827 (2008)

[37] Tang, Y. -W., Guilloteau, S., Piétu, V., et al., A&A **547**, A84 (2012)

[38] Tang, Y. -W., Guilloteau, S., Durtey, A., et al., ApJ **84**, 32 (2017)

[39] Vastel, C., Quénard, D., Le Gal, R., et al., MNRAS, 478, 5514 (2018)

[40] Vidal, T. H. G., Loison, J.-C., Jaziri, A. Y., et al., MNRAS, 469, 435 (2017)

[41] Wakelam, V., Ruaud, M., Hersant, F., et al., A&A **594**, A35 (2016)

[42] Walsh, C., Daley, C., Facchini, S., Juhász, A., A&A, 697, A114 (2017)

[43] Zhang, K., Crockett, N., Salyk, C., et al. ApJ, 805, 55, (2015)